Chemistry Faculty Research & Creative Works   Chemistry

15 Sep 2022

Understanding the Effect of Sodium Polyphosphate on Improving the Chemical Stability of Ti3c2tz Mxene in Water

Shuohan Huang

Varun Natu

Jingyi Tao

Yumin Xia

et. al. For a complete list of authors, see *https://scholarsmine.mst.edu/chem_facwork/3171*

Follow this and additional works at: https://scholarsmine.mst.edu/chem_facwork

Part of the Chemistry Commons

Recommended Citation

Check for updates

Understanding the effect of sodium polyphosphate on improving the chemical stability of $Ti_3C_2T_z$ MXene in water†

Shuohan Huang, [iD] *[ab] Varun Natu,[cd] Jingyi Tao, [iD] [a] Yumin Xia, [iD] [a] Vadym N. Mochalin [iD] *[be] and Michel W. Barsoum [iD] *[c]

Degradation of MXenes in aqueous environments severely limits the application and industrialization of this large family of two-dimensional (2D) materials. Hydrolysis and oxidation are now considered as two main degradation mechanisms and while significant efforts have been directed to prolonging the shelf-life of MXenes, separating and studying their degradation mechanisms have lagged behind. Herein, gas analysis *via* gas chromatography and Raman spectroscopy were used to investigate the effect of sodium polyphosphate, PP, on the degradation of $Ti_3C_2T_z$ MXene. Transmission and scanning electron microscopies, as well as X-ray photoelectron spectroscopywere also used as complimentary techniques to support conclusions derived from gas analysis and to confirm the extent of degradation *via* characterization of solid reaction products. Based on these studies we have determined that the addition of PP to an equal mass of $Ti_3C_2T_z$ solution can effectively suppress hydrolysis and protect $Ti_3C_2T_z$ from degradation.

1. Introduction

Transition metal carbides/nitrides (MXenes) with a general formula $M_{n+1}X_nT_z$ where $n = 1$–4, M is an early transition metal (*e.g.* Ti, Nb, V, Ta), X – carbon and/or nitrogen, and T stands for surface terminations (–OH, –F, and –O–) whose fraction (z) in the formula is unknown, but usually close to 2, constitute a large and growing family of two-dimensional (2D) materials.[1–3] The combination of hydrophilicity with high electrical conductivity provided by MXenes is unique among 2D materials.[2,4] Similar to their more known counterparts, bulk transition metal carbides, MXenes offer high elastic properties[5–7] and bending rigidity,[8] extra-low coefficient of friction achieving the superlubric regime[9], and attractive adhesive properties.[10,11] Because of their 2D structure and extraordinary properties, MXenes have attracted significant interest for many

applications such as optoelectronic devices,[12–14] triboelectric nanogenerators,[15] supercapacitors,[4,16,17] lithium ion batteries,[18,19] lithium–sulfur batteries,[20,21] lasers,[22] sensors,[23–25] solid lubricants,[9,26] THz wave transmission and communication technology,[13,27] among others.

However, it is well known that MXenes degrade when exposed to water and/or oxygen, the final result of which is their spontaneous transformation into the corresponding transition metal oxides.[28–32] Several methods have been proposed to suppress their degradationduring storage. Nicolosi *et al.* proposed refrigeration and de-aerated environment to substantially improve shelf life of $Ti_3C_2T_z$ and Ti_2CT_z MXenes in aqueous colloidal solutions.[31] Freezing of MXene solutions at low temperatures (below −20 °C) was also considered as an efficient way to reduce the degradation.[33,34] Zhao *et al.* have demonstrated that sodium L-ascorbate, used as antioxidant, can effectively protect MXenes from oxidation.[35] As more applications rely on the robust performance of MXenes, more attention is focused on extending their shelf life. Gogotsi *et al.* demonstrated that the modified synthesis method (changing the composition of TiC : Ti : Al = 2 : 1 : 1 from molar ratio to mass ratio) produced a less defective Ti_3AlC_2 MAX phase because of excess of Al in the starting mix, resulting in a more oxidation resistant $Ti_3C_2T_z$ MXene.[36] Koo *et al.* have found that $Ti_3C_2T_z$ MXene decomposed faster in acidic environments than in basic environments.[37] Kim *et al.* and Wang *et al.* also reported deep eutectic solvents (DESs) and salt solutions with high hydration enthalpies (*e.g.* saturated LiCl solutions), respectively, as efficient agents to suppress MXene degradation.[38,39]

[a]State Key Laboratory for Modification of Chemical Fibers and Polymer Materials, College of Materials Science and Engineering, Donghua University, Shanghai 201620, China. E-mail: huangs@dhu.edu.cn

[b]Department of Chemistry, Missouri University of Science & Technology, Rolla, MO 65409, USA. E-mail: mochalinv@mst.edu

[c]Department of Materials Science and Engineering, Drexel University, Philadelphia, PA 19104, USA. E-mail: barsoumw@drexel.edu

[d]National Chemical Laboratory (CSIR-NCL), Dr Homi Bhabha Road, Pune 411008, India

[e]Department of Materials Science & Engineering, Missouri University of Science & Technology, Rolla, MO 65409, USA

† Electronic supplementary information (ESI) available. See **https://doi.org/10.1039/d2ta04009c**

Using analysis of gaseous products, we previously experimentally demonstrated that hydrolysis is one of the main factors leading to MXene degradation in aqueous colloids.[40–42] Since then, hydrolysis and oxidation were considered as parallel processes contributing to MXene degradation. According to previous publications, MXene degradation starts from the edges and defects of the flakes.[43] Based on this hypothesis, Natu *et al.* further demonstrated that the positively charged edges of MXene flakes could be capped using polyanions: polyphosphates, PP, polysilicates, and polyborates, thus suppressing MXene degradation.[44,45] The addition of antioxidants can reduce the oxidation of MXenes, while application of low storage temperature in general suppresses all involved reactions (including hydrolysis and oxidation). However, it is not trivial to distinguish which route is suppressed more upon the addition of polyanions. To further investigate the mechanisms of polyanion-mediated suppression of MXene degradation, one can measure the carbon-containing gaseous products of the degradation because hydrolysis yields methane, while oxidation is expected to form carbon oxides.[37]

In this work, we studied hydrolysis and oxidation, as two possible routes of $Ti_3C_2T_z$ MXene degradation, upon addition of sodium polyphosphate (PP) *via* gas chromatography (GC) and Raman spectroscopy. The degradation kinetics of $Ti_3C_2T_z$ in water, with different concentrations of PP, under air or Ar atmospheres were also investigated. Additionally, TEM and SEM imaging, as well as XPS, XRD, and Raman of the resulting solids were used to characterize $Ti_3C_2T_z$ and its solid degradation products.

2. Experimental

2.1 MAX phase powder

Ti_3AlC_2 powder was made by mixing titanium carbide (Alfa Aesar, 99.5%, 2 μm), Al (Alfa Aesar, 99.5%, −325 mesh), and Ti (Alfa Aesar, 99.5%, −325 mesh), powders in a molar ratio 2 : 1.05 : 1, respectively. The powder mixture was ball milled (U.S. Stoneware) for 24 h at 70 rpm using zirconia balls under ambient air in polypropylene bottles and then transferred to an alumina boat, placed inside a tube furnace, and heated under argon (Ar) (flow rate 15 SSCM) to 1480 °C for 2 h followed by cooling to room temperature (RT) also under an Ar atmosphere. The heating and cooling rates were set at 5 °C min^{-1}. The resulting loosely sintered block was ground using a milling bit on a drill press and the milled powder was further sieved through a 400 mesh sieve (particle size < 38 μm).

2.2 MXene synthesis

First, 1 g of LiF (Alfa Aesar, 99.5%, 325 mesh) was dissolved in 10 ml of 12 M HCl (Fisher Scientific), afterwards 1 g of the sieved Ti_3AlC_2 powder was slowly added to the solution and stirred for 24 h at 35 °C and 300 rpm. The slurry was transferred into a plastic centrifuge tube and de-ionized (DI) water was added to 50 ml. The tube was then centrifuged at 3500 rpm for 2 min, and the clear supernatant was discarded. This washing step was repeated several times with fresh water until the pH of the

solution reached ≈7, at which point DI water was again added to the resulting MXene sediment and the suspension was bath sonicated while bubbling Ar for 1 h. The bath temperature was kept below 20 °C with ice to suppress oxidation/hydrolysis. The solution was then centrifuged for 1 h at 3500 rpm and the supernatant was separated for further use. The concentration of delaminated MXene in the supernatant was determined by vacuum filtering a known volume of the solution and measuring the weight of the resulting free standing MXene film after drying in a vacuum oven at 100 °C overnight.

2.3 Preparation of MXene samples for degradation studies

To investigate the effect of PP on $Ti_3C_2T_z$ degradation, we diluted and divided the as-prepared concentrated MXene suspension (∼7.5 mg ml^{-1}) into 6 parts of 6 ml each in 10 ml glass vials. The gas phase in the vials was either air or Ar. The samples were labelled as $Ti_3C_2T_z$–air (no PP added, no Ar purging), $Ti_3C_2T_z$–Ar (no PP added, purged with Ar for 15 min), and $Ti_3C_2T_z$–PP (30 μl of 1 M PP solution added, no Ar purging). The samples were prepared in duplicates, one was stored at 70 °C to accelerate the degradation while the other was stored at RT for slower degradation and better monitoring of the morphological changes in the 2D flakes.

Another batch of $Ti_3C_2T_z$ was prepared to optimize the amount of PP added in order to suppress its degradation. The as prepared $Ti_3C_2T_z$ suspension (∼15 mg ml^{-1}) was diluted to ∼2.5 mg ml^{-1} and mixed with different proportions of PP by weight to yield: $Ti_3C_2T_z$–5PP (MXene : PP = 1 : 5), $Ti_3C_2T_z$–1PP (MXene : PP = 1 : 1), $Ti_3C_2T_z$–0.2PP (MXene : PP = 5 : 1), $Ti_3C_2T_z$–0.005PP (MXene : PP = 1 : 0.005), $Ti_3C_2T_z$–Ar, and $Ti_3C_2T_z$–air. In these sample names XPP indicates mass ratio between $Ti_3C_2T_z$ and PP. The ratio 1 : 0.005 was chosen as the minimal amount of PP necessary to cap the edges of typical MXene particles, according to calculations based on the PP chain length and the perimeter of a typical MXene flake (Fig. S5 and calculation details are shown in ESI†). Again, the samples were prepared in duplicates, half stored at 70 °C and half at RT.

Sodium PP (Acros Organics, pure) was used as received. Ar gas (UHP300, Airgas) used in this work was 99.999% pure.

2.4 Characterization

Raman spectra of the gas phase above the colloids were recorded through the glass vial wall, without opening the vial, using a 532 nm laser with 1200 lines/mm grating, 5× objective, 20 s exposure time, 100% of laser power, and 10 accumulations. Raman spectra of the solids were recorded using a 532 nm laser with 2400 lines/mm grating, 50× objective, 10 s exposure time, 10% of laser power, and 10 accumulations. Raman spectra were collected with a Renishaw InVia confocal Raman microspectrometer.

The gases collected from MXene degradation were analyzed with a gas chromatograph (GC, Thermal Scientific Trace-1300) equipped with a fused silica capillary column (Carboxen 1006 PLOT, length 30 m, diameter 0.53 mm and 30 μm thickness) and a thermal conductivity detector (TCD). Helium, He, was used as the carrier and reference gas. The flow rates were 4 and

This journal is © The Royal Society of Chemistry 2022

J. Mater. Chem. A, 2022, **10**, 22016–22024 | **22017**

4.3 ml min^{-1}, respectively. The purge flow of He was 5 ml min^{-1}. The oven, TCD detector, and TCD filament temperatures were held at 35, 230, and 280 °C, respectively. For each measurement, 0.1 ml of gas was manually injected into the GC unit with a 1 ml gastight syringe (Hamilton).

Transmission electron microscope (TEM) images of $Ti_3C_2T_z$ degraded in different environments were acquired on a JEM 2100 (JEOL, Ltd) TEM at an accelerating voltage of 200 kV. To remove the PP from the samples before TEM imaging, the $Ti_3C_2T_z$–PP suspension was washed 2 times using DI water, centrifuged at 5000 rpm, and re-dispersed in DI water before measurements. Finally, the TEM sampleswere prepared by depositing 5 μl of this diluted $Ti_3C_2T_z$ suspension onto copper TEM grids (Electron Microscopy, China).

XPS (ESCALAB 250Xi, Thermo Scientific) equipped with an Al Kα source (1486.6 eV) was used for characterization of MXenes and the solid products of their degradation. The binding energy was calibrated based on C 1s line (binding energy 284.8 eV). Charge neutralization was applied. No sputtering was used for the measurements.

Solid products of MXenes were characterized using powder X-ray diffraction (XRD, D8 Advance, Bruker) with Cu Kα radiation ($\lambda = 1.5406$ Å) at $U = 40$ kV and $I = 40$ mA.

Scanning electron microscope (SEM) imaging for $Ti_3C_2T_z$, degraded in different environments, was carried out on a Hitachi SU8010 SEM at a 10 kV accelerating voltage and a 10 μA current. Prior to imaging, PP containing MXene samples were washed 2 times using DI water to remove the PP, centrifuged at 5000 rpm, and re-dispersed in DI water. The SEM samples were prepared by drop casting 10 μl of this $Ti_3C_2T_z$suspension on a Si wafer.

3. Results and discussion

Direct analysis of the evolved gas products, by well-established sensitive analytical chemistry techniques, provides probably the best way to monitor MXene degradation.[41] It is unambiguous because carbon containing gaseous products directly correspond to the fraction of degraded MXene in the sample, whereas different oxidation states of transition metal, typically detected with XPS by deconvolution of the corresponding overlapping peaks, may correspond to fully or partially degraded MXene flakes. Similarly, analysis of solids by Raman spectroscopy and XRD is not as easily interpretable as chromatography results, and does not directly provide the fraction of decomposed MXene in the sample. These characterization techniques are also inferior to gas chromatography in terms of sensitivity. In our previous studies we showed that the main component of the gas formed due to $Ti_3C_2T_z$ degradation was CH_4, which is the carbon-containing product of MXene hydrolysis.[40] Following these earlier results, here we monitored $Ti_3C_2T_z$ degradation by measuring CH_4 evolution over time. Fig. 1a shows a schematic of the Raman spectroscopy setup for quantifying the gaseous products of degradation without ever
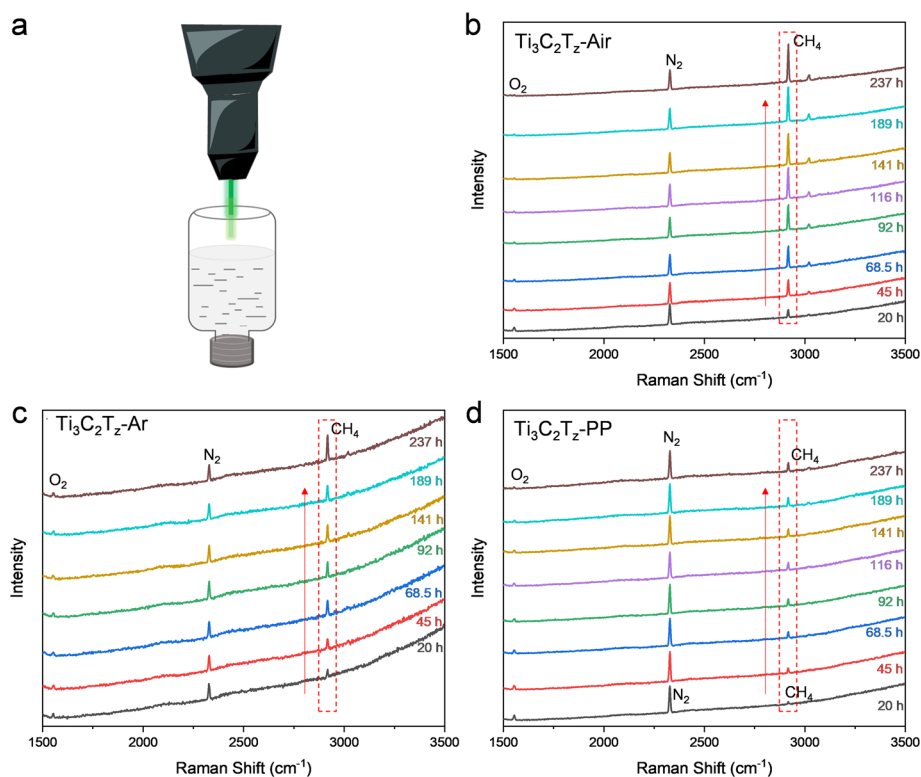

Fig. 1 (a) Schematic of Raman spectroscopy detection of gaseous products of $Ti_3C_2T_z$ degradation in colloidal solution without opening the reaction vial. Raman spectra of gas phases collected from (b) $Ti_3C_2T_z$–air, (c) $Ti_3C_2T_z$–Ar, and (d) $Ti_3C_2T_z$–PP samples degraded in glass vials over time indicated on plots.
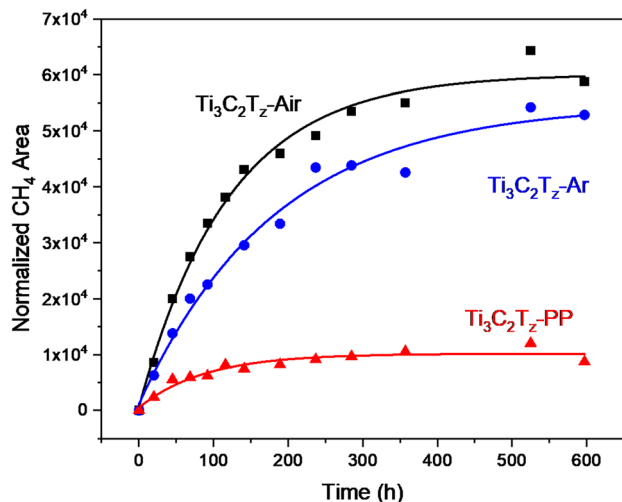
22018 | *J. Mater. Chem. A*, 2022, **10**, 22016–22024

This journal is © The Royal Society of Chemistry 2022

Fig. 2 Degradation kinetics of $Ti_3C_2T_z$–air, $Ti_3C_2T_z$–Ar, and $Ti_3C_2T_z$–PP samples at 70 °C as measured by Raman spectroscopy.

opening the glass reaction vial. The suspensions were stored in a 70 °C oven to accelerate the reaction except the time when they were extracted and cooled down to RT for a few minutes to record the Raman spectra of the gas phase. The accumulation of CH_4 over time was monitored by integration of the Raman peak corresponding to the C–H stretch vibrations at ~2918 cm^{-1}. The Raman spectra collected from gas phase of $Ti_3C_2T_z$–air, $Ti_3C_2T_z$–Ar, and $Ti_3C_2T_z$–PP in glass vials over time are shown in Fig. 1b–d. The N_2 and O_2 peaks in the $Ti_3C_2T_z$–air and $Ti_3C_2T_z$–PP samples (Fig. 1b and d) originate from air in the vials and in the space between the vials and the lens of the spectrometer. The least intense N_2 peaks were observed in the $Ti_3C_2T_z$–Ar sample since in this case these peaks originate only from the air in the gap between vial and lens. The increasing intensity of CH_4 peaks over time is observed for all samples, indicating progress of the hydrolysis reaction. However, the intensities of the CH_4 peaks in the $Ti_3C_2T_z$–air sample increase faster compared to other samples. In contrast, the increase in intensities of the CH_4 peak in the $Ti_3C_2T_z$–PP vial is the slowest compared to other samples.

The kinetics of degradation of $Ti_3C_2T_z$–air, $Ti_3C_2T_z$–Ar, and $Ti_3C_2T_z$–PP samples based on their Raman spectra are summarized in Fig. 2. The results were fit to an exponential growth function, *viz.*

$$A(t) = A_0 - A_\infty e^{-(t/\tau)} \quad (1)$$

where A_∞ is the maximum value of the CH_4 peak area corresponding to fully hydrolysed MXene (*i.e.*, at $t \to \infty$), A_0 is the offset, $A(t)$ is the area of CH_4 peak recorded at time t, and the time constant τ is inversely proportional to an apparent rate constant of degradation. The fitting parameters for all samples are listed in ESI.† Not surprisingly, at a given time more CH_4 was produced from the $Ti_3C_2T_z$–air sample ($\tau = 120 \pm 10$ h) than the $Ti_3C_2T_z$–Ar ($\tau = 182 \pm 22$ h), indicating that hydrolysis is faster in the presence of oxygen. The amplitudes A_∞ of $Ti_3C_2T_z$–air (60 000 ± 2000) and $Ti_3C_2T_z$–Ar (54 000 ± 2000) samples,

corresponding to the maximum area of CH_4 peak, are similar, which means the complete degradation of MXene in both air and Ar environments produces similar amounts of CH_4, *i.e.*, C atoms of MXene end up mainly in CH_4, not carbon oxides, and thus, hydrolysis dominates the degradation. However, the $A_\infty = 9700 \pm 900$, obtained from fitting of the $Ti_3C_2T_z$–PP curve, is considerably smaller compared with the other two samples which did not contain PP, thus indicating that the addition of PP is effective in suppressing hydrolysis.

After complete degradation of the samples, the gas phases were analyzed by GC with TCD. Fig. 3 shows chromatograms of gaseous products collected after complete degradation of $Ti_3C_2T_z$–air, $Ti_3C_2T_z$–Ar, and $Ti_3C_2T_z$–PP samples. Mainly CH_4 is detected for $Ti_3C_2T_z$ in either air or Ar atmosphere with a small amount of CO_2. The relative integrated area of the CO_2 peak in ambient air is ~0.05%, while in the gaseous phase of $Ti_3C_2T_z$–air and $Ti_3C_2T_z$–Ar this area is 0.06–0.08%, indicating that only a small amount of CO_2 is formed during $Ti_3C_2T_z$ degradation in water under eitherair or an Ar atmosphere without PP addition. Since CO_2 is a product of MXene oxidation while CH_4 is the hydrolysis product, this result also illustrates the dominant role of MXene hydrolysis in the process of its degradation in aqueous colloids. However, CH_4 peak for $Ti_3C_2T_z$–PP is much less intense and the intensity of the CO_2 peak is higher, resulting in larger $CO_2 : CH_4$ ratios of peak intensities compared with chromatograms of either $Ti_3C_2T_z$–air or $Ti_3C_2T_z$–Ar, again indicating that PP addition mostly suppressed hydrolysisrather than oxidation. To summarize this section, Raman and GC demonstrate that the addition of PP considerably reduces the rate of hydrolysis but has less of an effect on the oxidation of $Ti_3C_2T_z$. It should also be noted that as the

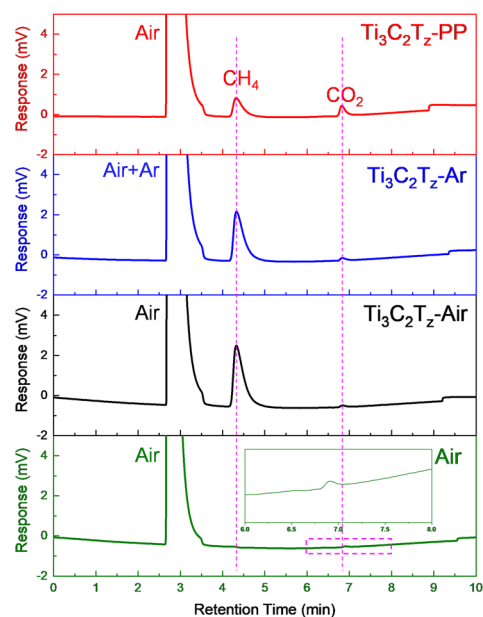**Fig. 3** Gas chromatograms of ambient air and gaseous products collected from $Ti_3C_2T_z$–air, $Ti_3C_2T_z$–Ar, and $Ti_3C_2T_z$–PP samples after their complete degradation at 70 °C. Dashed pink lines indicate the peak positions of CH_4 and CO_2. Dashed rectangle in the bottom panel indicates the area represented in more detail by the inset in this panel.
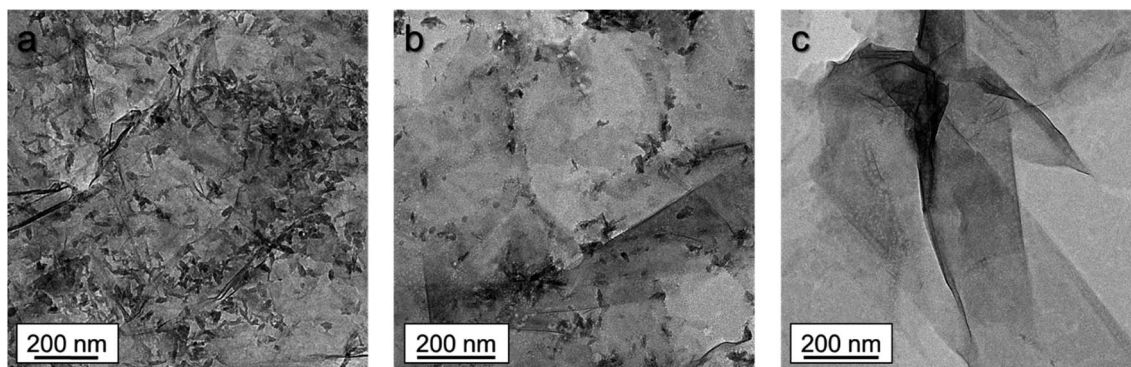
This journal is © The Royal Society of Chemistry 2022

J. Mater. Chem. A, 2022, **10**, 22016–22024 | **22019**

Fig. 4 TEM images of MXene flakes from (a) $Ti_3C_2T_z$–air, (b) $Ti_3C_2T_z$–Ar, and (c) $Ti_3C_2T_z$–PP samples stored at RT over ~20 days.

experiments were carried out at 70 °C, MXene degradation rates are significantly higher than at RT.

A duplicate set of $Ti_3C_2T_z$–air, $Ti_3C_2T_z$–Ar, and $Ti_3C_2T_z$–PP samples was stored at RT to observe the changes in MXene morphology over time (Fig. 4). At the end of this experiemnt, the entire surface of the MXene flakes from $Ti_3C_2T_z$–air sample is covered by TiO_2 nanoparticles (Fig. 4a) due to severe degradation. The flakes from the $Ti_3C_2T_z$–Ar sample (Fig. 4b) show TiO_2 particles mainly along the edges, a consequence of a slower and milder MXene oxidation/hydrolysis in the absence of oxygen. However, when PP was added, the MXene flakes remained largely intact over ~20 days storage time (Fig. 4c), showing morphology similar to the freshly made $Ti_3C_2T_z$ MXene flakes (Fig. S1†). Thus, suppression of hydrolysis by PP can largely protect MXene from degradation, even in the presence of air. This again demonstrates that hydrolysis is a crucial process in MXene degradation.[40]

Encouraged by the results above, we moved ahead to determine the optimal concentration of PP needed to protect $Ti_3C_2T_z$ from degradation. Samples with different mass ratios of MXene : PP ($Ti_3C_2T_z$–5PP, $Ti_3C_2T_z$–1PP, $Ti_3C_2T_z$–0.2PP, and $Ti_3C_2T_z$–0.005PP) were studied. Samples $Ti_3C_2T_z$–Ar and $Ti_3C_2T_z$–air

without added PP were also prepared for comparison purposes. Fig. 5a shows the changes in the visual appearance of the MXene suspensions in different environments over time at 70 °C. According to the photographs, $Ti_3C_2T_z$–0.005PP and $Ti_3C_2T_z$–air samples both degrade within 185 h, implying that very small amounts of PP added make no difference compared with the control samples. Purging with Ar prolongs the shelf life of MXene compared to the control, however $Ti_3C_2T_z$–Ar sample has completely degraded over 280 h. Although it seems that a larger amount of PP suppresses the degradation of MXenes better at 280 h, photographs acquired at 375 h show that both $Ti_3C_2T_z$–5PP and $Ti_3C_2T_z$–0.2PP have completely degraded. However, the $Ti_3C_2T_z$–1PP sample showed no visual signs of degradation at 375 h (end of experiment). It is worth noting that MXene flakes in $Ti_3C_2T_z$–5PP sample (the highest concentration of PP studied) precipitate after 185 h storage at 70 °C (Fig. S2†), but can be re-dispersed with shaking (Fig. 5a). PP, especially in high concentrations precipitates MXene flakes (a known salting-out effect), which can slow down diffusion processes. But, as Fig. 5 shows, precipitation-induced effects cannot protect MXene from degradation to the same extent as the proper (lower) concentration of PP, which is achieved at a 1 : 1
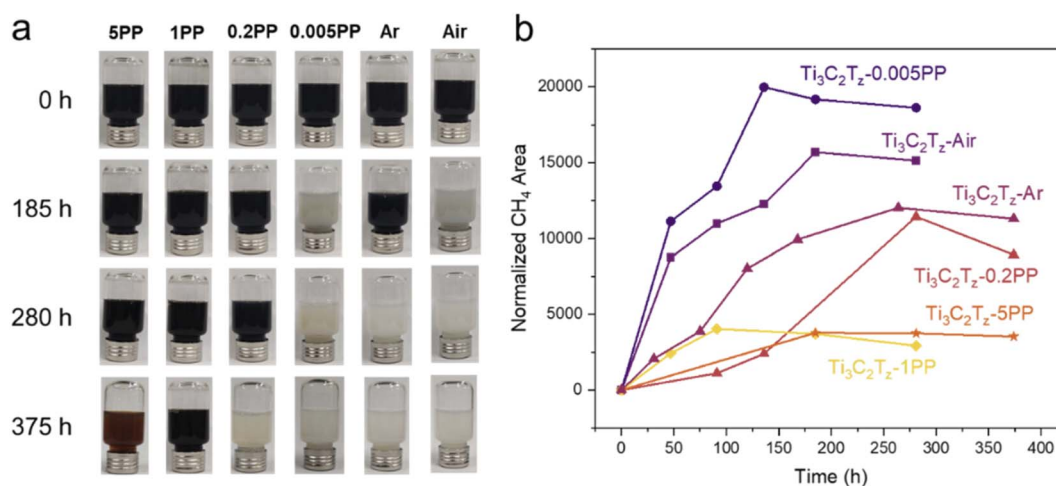

Fig. 5 (a) Optical photographs of $Ti_3C_2T_z$ MXene in different environments over time. (b) Amount of methane (measured by Raman spectroscopy) accumulated during the degradation of $Ti_3C_2T_z$ MXene in different environments over time.

Table 1 Areas of peaks corresponding to main gaseous products of MXene degradation and ambient air, as measured by GC

Samples	CH_4 area (mV min)	CO_2 area (mV min)	CO_2 percent area (%)
$Ti_3C_2T_z$–5PP (MXene : PP = 1 : 5)	0.286	0.107	0.58
$Ti_3C_2T_z$–1PP (MXene : PP = 1 : 1)	0.258	0.079	0.40
$Ti_3C_2T_z$–0.2PP (MXene : PP = 5 : 1)	0.857	0.018	0.07
$Ti_3C_2T_z$–0.005PP (MXene : PP = 1 : 0.005)	1.035	0.013	0.07
$Ti_3C_2T_z$–Ar	0.876	0.013	0.08
$Ti_3C_2T_z$–air	0.880	0.013	0.06
Air	0	0.009	0.05

mass ratio. Therefore, this observation clearly demonstrates that PP indeed suppresses the chemical reactions of MXene degradation, instead of hindering diffusion processes. We hypothesize that the suppression of MXene hydrolysis by PP is mainly due to a combination of two factors: (i) as explained in some of our previous publications, the positively charged MXene flake edges are capped by negatively charged PP anions, which can protect the flake edges from the attack by water molecules;[45] (ii) sodium polyphosphate ions, same as many other electrolytes, are known to reduce the activity of water in solution. Reduced water activity slows down the kinetics of hydrolysis.[38,39]

In addition to GC, we have analyzed the head space of the 6 samples using Raman spectroscopy. The main advantage of Raman spectroscopy compared to GC in our study is that it allows to monitor gas composition of the samples through the walls of the vials without ever opening them or taking any gas aliquots out. The kinetics of degradation of all 6 samples based on the corresponding CH_4 peak area are plotted in Fig. 5b.

These data show a trend similar to the changes in visual appearance (Fig. 5a). Less CH_4 is produced from $Ti_3C_2T_z$–5PP, $Ti_3C_2T_z$–1PP, and $Ti_3C_2T_z$–0.2PP samples compared with the samples containing no, or less, PP added ($Ti_3C_2T_z$–0.005PP, $Ti_3C_2T_z$–Ar, and $Ti_3C_2T_z$–air) due to hydrolysis suppression by the PP.

The gaseous products of 6 samples were further analyzed by GC when the degradation reactions come to an end (judging from the color of the suspensions) and the results are summarized in Table 1. These GC results are in line with the discussion above that PP reduces hydrolysis resulting in less CH_4 produced. The final CH_4 areas are 0.25–0.30 mV min for $Ti_3C_2T_z$–5PP and $Ti_3C_2T_z$–1PP, while for the other four samples, with low or no PP added, the areas are ~3 times larger, 0.85–1.03 mV min. At the same time, the amount of CO_2 produced during the degradation reflects the contribution of oxidative route. The CO_2 percent area (Table 1, last column) is calculated as a ratio of the CO_2 peak area to the sum of the peak areas of air, CH_4, and CO_2. The relative areas of the CO_2 peaks for the
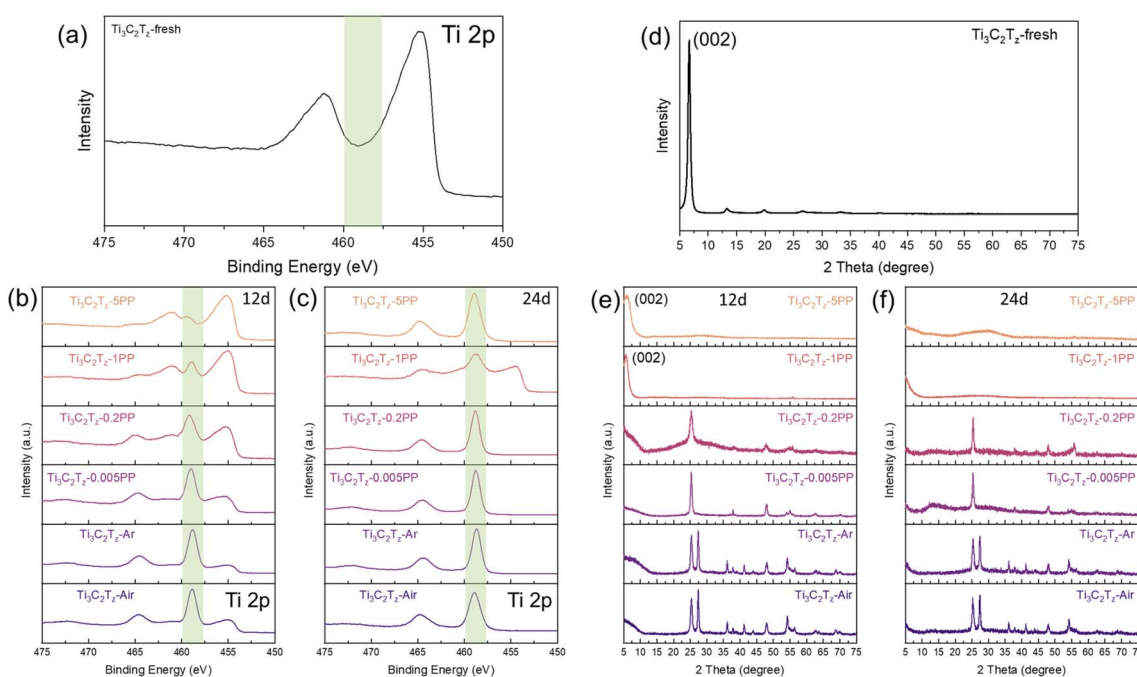

Fig. 6 High resolution XPS spectra in Ti 2p binding energy range for (a) fresh $Ti_3C_2T_z$ MXene, (b) $Ti_3C_2T_z$ MXene in different environments after 12 days, and (c) $Ti_3C_2T_z$ MXene in different environments after 24 days. XRD patterns of (d) fresh $Ti_3C_2T_z$ MXene, (e) $Ti_3C_2T_z$ MXene in different environments after 12 days, and (f) $Ti_3C_2T_z$ MXene in different environments after 24 days.
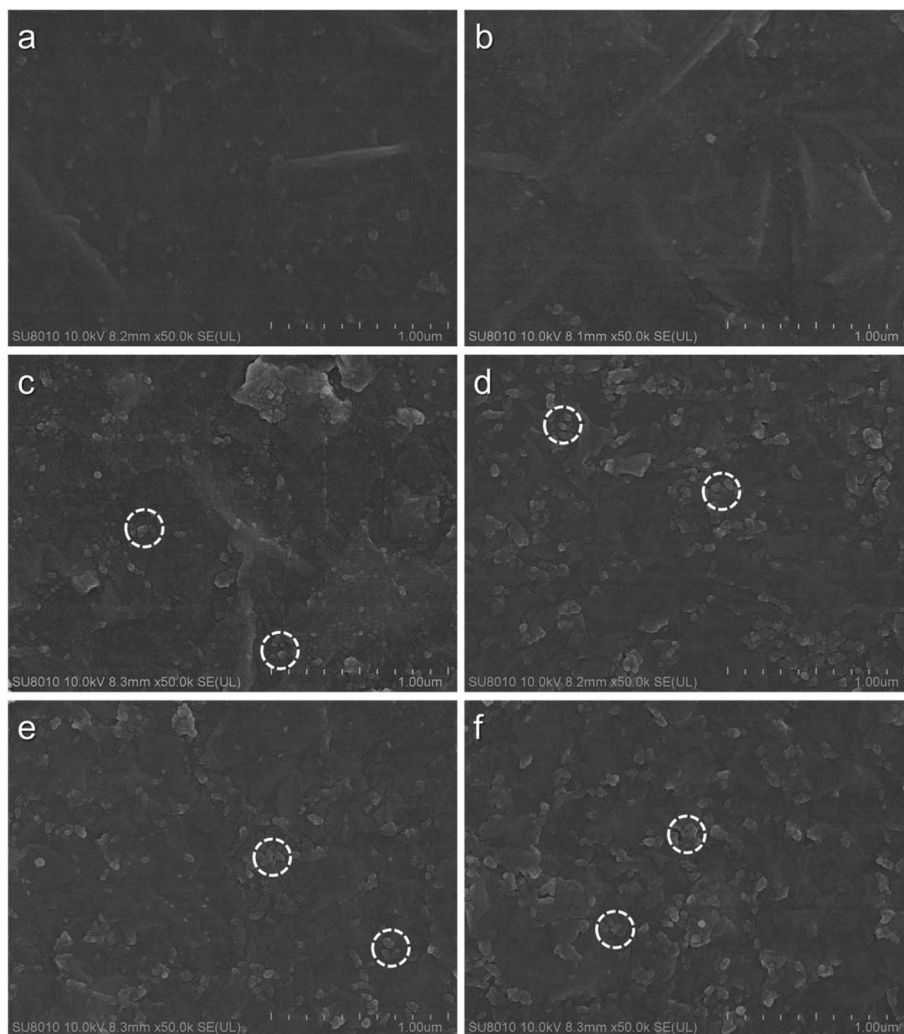
This journal is © The Royal Society of Chemistry 2022

J. Mater. Chem. A, 2022, **10**, 22016–22024 | **22021**

Fig. 7 SEM images of the solids dried from, (a) $Ti_3C_2T_z$–5PP, (b) $Ti_3C_2T_z$–1PP, (c) $Ti_3C_2T_z$–0.2PP, (d) $Ti_3C_2T_z$–0.005PP, (e) $Ti_3C_2T_z$–Ar, and (f) $Ti_3C_2T_z$–air samples stored at RT over time. Representative TiO_2 particles are highlighted by circles.

samples $Ti_3C_2T_z$–5PP and $Ti_3C_2T_z$–1PP are 5–10 times larger compared to the other four samples with low, or no, PP added. Thus, all results discussed above consistently point out to the inhibition of MXene hydrolysis by PP, with less or no effect of PP on MXene oxidation. The optimal amount of PP in terms of prolonging shelf life of $Ti_3C_2T_z$ MXene was determined to be MXene : PP = 1 : 1 by weight.

As mentioned above, gas analysis gives direct and unambiguous information about MXene degradation, which is sufficient to monitor its progress. However, to further support the results of gas analysis, solid products obtained after storing $Ti_3C_2T_z$ in different environments at 70 °C were analyzed using XPS and XRD (Fig. 6). The fresh $Ti_3C_2T_z$ shows two main peaks in the high-resolution Ti 2p spectra at ~455 and 462 eV, which can be assigned to Ti $2p_{3/2}$ and Ti $2p_{1/2}$ in $Ti_3C_2T_z$, respectively. The green band centered at ~459 eV highlights the binding energy associated with TiO_2, which, as expected, is not detectable in fresh $Ti_3C_2T_z$ (Fig. 6a). After 12 days, TiO_2 peak appears for all MXene samples but with varying intensity. After 12 days $Ti_3C_2T_z$–5PP shows the lowest extent of degradation among all samples,

may be because of diffusion limitations due to precipitation, slowing down the degradation on a shorter time scale. However, after 24 days, the Ti peak belonging to $Ti_3C_2T_z$ (a broad peak ~455 eV) can be detected only in $Ti_3C_2T_z$–1PP sample, while all other samples show TiO_2, confirming that the slowest degradation rate occurs in the $Ti_3C_2T_z$–1PP suspensions.

Not surprisingly, the XRD patterns also demonstrate similar trend. The fresh $Ti_3C_2T_z$ shows characteristic (002) peak of MXene. After 12 days, the (002) peak can still be detected in $Ti_3C_2T_z$–5PP and $Ti_3C_2T_z$–1PP samples, while other MXene samples ($Ti_3C_2T_z$–air, $Ti_3C_2T_z$–Ar, $Ti_3C_2T_z$–0.005PP, and $Ti_3C_2T_z$–0.2PP) show only TiO_2 signals. After 24 days, however, neither (002) peak of MXene nor TiO_2 peaks were detected for $Ti_3C_2T_z$–5PP and $Ti_3C_2T_z$–1PP samples. This may be because many defects have accumulated in the MXene structure by that time, breaking the long-range order in MXene stacks. It is interesting to note that $Ti_3C_2T_z$–air and $Ti_3C_2T_z$–Ar samples show the formation of both rutile and anatase during the degradation of MXenes, while only anatase can be detected with the addition of PP even when the PP : MXene ratio is as low as

0.005. Raman spectra of solids acquired after the degradation of different samples also confirmed the aforementioned conclusions (Fig. S3†).

SEM micrographs for the 6 samples stored at RT for ~30 days are shown in Fig. 7. The image of the fresh MXene is shown in Fig. S4.† Consistent with the visual appearance (Fig. 5a) and Raman results (Fig. 5b), the amount of TiO_2 observed in these micrographs follows the trend: $Ti_3C_2T_z$–air $\approx$ $Ti_3C_2T_z$–0.005PP > $Ti_3C_2T_z$–Ar > $Ti_3C_2T_z$–0.2PP > $Ti_3C_2T_z$–5PP > $Ti_3C_2T_z$–1PP, further confirming that when PP is added to the aqueous MXene colloid in a 1 : 1 mass ratio it results in the best protection against degradation.

4. Conclusions

In summary, $Ti_3C_2T_z$ MXene degradation in water without, and with, the addition of sodium polyphosphate was studied by analyzing the evolved gases with Raman spectroscopy and gas chromatography, complemented by visual observations, SEM and TEM imaging, as well as XPS, XRD, and Raman spectroscopy of the resulting solids. The kinetics of MXene hydrolysis was measured from the data on the composition of gaseous degradation products. The results show that the addition of PP significantly suppresses the hydrolysis of $Ti_3C_2T_z$ but has less, to no, effect on its oxidation. The long-term chemical stability of $Ti_3C_2T_z$ was achieved by adding PP in a 1 : 1 mass ratio to the aqueous MXene colloid.

This work also illustrates an effective and useful method for the separation of the two main processes leading to MXene degradation in aqueous environments (hydrolysis *vs.* oxidation). We believe that our findings and experimental techniques reported herein will be important for further understanding of MXene chemistries, stabilities, and applications, and will have broader impact in the area of chemistry of other 2D materials as well.

Conflicts of interest

There are no conflicts to declare.

Acknowledgements

Notes and references

1 M. Naguib, M. Kurtoglu, V. Presser, J. Lu, J. J. Niu, M. Heon, L. Hultman, Y. Gogotsi and M. W. Barsoum, *Adv. Mater.*, 2011, **23**, 4248–4253.

2 M. Naguib, V. N. Mochalin, M. W. Barsoum and Y. Gogotsi, *Adv. Mater.*, 2014, **26**, 992–1005.

3 A. VahidMohammadi, J. Rosen and Y. Gogotsi, *Science*, 2021, **372**, eabf1581.

4 M. Ghidiu, M. R. Lukatskaya, M. Q. Zhao, Y. Gogotsi and M. W. Barsoum, *Nature*, 2014, **516**, 78–81.

5 V. N. Borysiuk, V. N. Mochalin and Y. Gogotsi, *Nanotechnology*, 2015, **26**, 265705.

6 A. Lipatov, H. Lu, M. Alhabeb, B. Anasori, A. Gruverman, Y. Gogotsi and A. Sinitskii, *Sci. Adv.*, 2018, **4**, eaat0491.

7 N. Zhang, Y. Hong, S. Yazdanparast and M. A. Zaeem, *2D Mater.*, 2018, **5**, 045004.

8 V. N. Borysiuk, V. N. Mochalin and Y. Gogotsi, *Comput. Mater. Sci.*, 2018, **143**, 418–424.

9 S. Huang, K. Mutyala, A. Sumant and V. Mochalin, *Mater. Today Adv.*, 2021, **9**, 100133.

10 Y. Li, S. Huang, C. Wei, C. Wu and V. N. Mochalin, *Nat. Commun.*, 2019, **10**, 1–8.

11 Y. Li, S. Huang, C. Wei, D. Zhou, B. Li, C. Wu and V. N. Mochalin, *ACS Appl. Mater. Interfaces*, 2021, **13**, 4682–4691.

12 K. Montazeri, M. Currie, L. Verger, P. Dianat, M. W. Barsoum and B. Nabet, *Adv. Mater.*, 2019, **31**, 1903271.

13 K. Chaudhuri, M. Alhabeb, Z. Wang, V. M. Shalaev, Y. Gogotsi and A. Boltasseva, *ACS Photonics*, 2018, **5**, 1115–1122.

14 Y. Dong, S. Chertopalov, K. Maleski, B. Anasori, L. Hu, S. Bhattacharya, A. M. Rao, Y. Gogotsi, V. N. Mochalin and R. Podila, *Adv. Mater.*, 2018, **30**, 1705714.

15 Y. Dong, S. S. K. Mallineni, K. Maleski, H. Behlow, V. N. Mochalin, A. M. Rao, Y. Gogotsi and R. Podila, *Nano Energy*, 2018, **44**, 103–110.

16 M. R. Lukatskaya, O. Mashtalir, C. E. Ren, Y. Dall'Agnese, P. Rozier, P. L. Taberna, M. Naguib, P. Simon, M. W. Barsoum and Y. Gogotsi, *Science*, 2013, **341**, 1502–1505.

17 C. Zhang, M. P. Kremer, A. Seral-Ascaso, S. H. Park, N. McEvoy, B. Anasori, Y. Gogotsi and V. Nicolosi, *Adv. Funct. Mater.*, 2018, **28**, 1705506.

18 M. Naguib, J. Halim, J. Lu, K. M. Cook, L. Hultman, Y. Gogotsi and M. W. Barsoum, *J. Am. Chem. Soc.*, 2013, **135**, 15966–15969.

19 Y. Xie, M. Naguib, V. N. Mochalin, M. W. Barsoum, Y. Gogotsi, X. Yu, K. W. Nam, X. Q. Yang, A. I. Kolesnikov and P. R. Kent, *J. Am. Chem. Soc.*, 2014, **136**, 6385–6394.

20 R. Pai, V. Natu, M. Sokol, M. Carey, M. W. Barsoum and V. Kalra, *Cell Rep. Phys. Sci.*, 2021, **2**, 100480.

21 H. Tang, W. Li, L. Pan, C. P. Cullen, Y. Liu, A. Pakdel, D. Long, J. Yang, N. McEvoy and G. S. Duesberg, *Adv. Sci.*, 2018, **5**, 1800502.

22 J. Yi, L. Du, J. Li, L. Yang, L. Hu, S. Huang, Y. Dong, L. Miao, S. Wen, V. N. Mochalin, C. Zhao and A. M. Rao, *2D Mater.*, 2019, **6**, 045038.

23 S. Chertopalov and V. N. Mochalin, *ACS Nano*, 2018, **12**, 6109–6116.

This journal is © The Royal Society of Chemistry 2022

J. Mater. Chem. A, 2022, **10**, 22016–22024 | **22023**

24 S. J. Kim, H. J. Koh, C. E. Ren, O. Kwon, K. Maleski, S. Y. Cho, B. Anasori, C. K. Kim, Y. K. Choi, J. Kim, Y. Gogotsi and H. T. Jung, *ACS Nano*, 2018, **12**, 986–993.

25 S. Xu, Y. Dall'Agnese, G. Wei, C. Zhang, Y. Gogotsi and W. Han, *Nano Energy*, 2018, **50**, 479–488.

26 X. Yin, J. Jin, X. Chen, A. Rosenkranz and J. Luo, *ACS Appl. Mater. Interfaces*, 2019, **11**, 32569–32576.

27 G. Li, N. Amer, H. Hafez, S. Huang, D. Turchinovich, V. N. Mochalin, F. A. Hegmann and L. V. Titova, *Nano Lett.*, 2019, **20**, 636–643.

28 O. Mashtalir, K. M. Cook, V. N. Mochalin, M. Crowe, M. W. Barsoum and Y. Gogotsi, *J. Mater. Chem. A*, 2014, **2**, 14334–14338.

29 A. Lipatov, M. Alhabeb, M. R. Lukatskaya, A. Boson, Y. Gogotsi and A. Sinitskii, *Adv. Electron. Mater.*, 2016, **2**, 1600255.

30 K. Maleski, V. N. Mochalin and Y. Gogotsi, *Chem. Mater.*, 2017, **29**, 1632–1640.

31 C. Zhang, S. Pinilla, N. McEvoy, C. P. Cullen, B. Anasori, E. Long, S.-H. Park, A. Seral-Ascaso, A. Shmeliov, D. Krishnan, C. Morant, X. Liu, D. S. Duesberg, Y. Duesberg and V. Nicolosi, *Chem. Mater.*, 2017, **29**, 4848–4856.

32 J. Jiang, S. Bai, J. Zou, S. Liu, J.-P. Hsu, N. Li, G. Zhu, Z. Zhuang, Q. Kang and Y. Zhang, *Nano Res.*, 2022, **15**, 6551–6567.

33 Y. Chae, S. J. Kim, S.-Y. Cho, J. Choi, K. Maleski, B.-J. Lee, H.-T. Jung, Y. Gogotsi, Y. Lee and C. W. Ahn, *Nanoscale*, 2019, **11**, 8387–8393.

34 J. Zhang, N. Kong, D. Hegh, K. A. S. Usman, G. Guan, S. Qin, I. Jurewicz, W. Yang and J. M. Razal, *ACS Appl. Mater. Interfaces*, 2020, **12**, 34032–34040.

35 X. Zhao, A. Vashisth, E. Prehn, W. Sun, S. A. Shah, T. Habib, Y. Chen, Z. Tan, J. L. Lutkenhaus, M. Radovic and M. J. Green, *Matter*, 2019, **1**, 513–526.

36 T. S. Mathis, K. Maleski, A. Goad, A. Sarycheva, M. Anayee, A. C. Foucher, K. Hantanasirisakul, C. E. Shuck, E. A. Stach and Y. Gogotsi, *ACS Nano*, 2020, **15**(4), 6420–6429.

37 S. Doo, A. Chae, D. Kim, T. Oh, T. Y. Ko, S. J. Kim, D.-Y. Koh and C. M. Koo, *ACS Appl. Mater. Interfaces*, 2021, **13**, 22855–22865.

38 J. Kim, Y. Yoon, S. K. Kim, S. Park, W. Song, S. Myung, H. K. Jung, S. S. Lee, D. H. Yoon and K. S. An, *Adv. Funct. Mater.*, 2021, **31**, 2008722.

39 X. Wang, Z. Wang and J. Qiu, *Angew. Chem., Int. Ed.*, 2021, **60**, 26587–26591.

40 S. Huang and V. N. Mochalin, *Inorg. Chem.*, 2019, **58**, 1958–1966.

41 S. Huang and V. N. Mochalin, *ACS Nano*, 2020, **14**, 10251–10257.

42 S. Huang and V. N. Mochalin, *Inorg. Chem.*, 2022, **61**, 9877–9887.

43 F. Xia, J. Lao, R. Yu, X. Sang, J. Luo, Y. Li and J. Wu, *Nanoscale*, 2019, **11**, 23330–23337.

44 V. Natu, M. Sokol, L. Verger and M. W. Barsoum, *J. Phys. Chem. C*, 2018, **122**, 27745–27753.

45 V. Natu, J. L. Hart, M. Sokol, H. Chiang, M. L. Taheri and M. W. Barsoum, *Angew. Chem., Int. Ed.*, 2019, **131**, 12785–12790.

22024 | *J. Mater. Chem. A*, 2022, **10**, 22016–22024

This journal is © The Royal Society of Chemistry 2022